Digital Signal Processing 79 (2018) 57–65

Contents lists available at ScienceDirect

Digital Signal Processing

www.elsevier.com/locate/dsp

# OMP-based DOA estimation performance analysis

Mohammad Emadi [a,1], Ehsan Miandji [b,*,1], Jonas Unger [b]

[a] Qualcomm Technologies Inc., San Jose, CA, USA
[b] Department of Science and Technology, Linköping University, Sweden

ARTICLE INFO

*Article history:*
Available online 21 April 2018

*Keywords:*
Direction of arrival
Orthogonal Matching Pursuit (OMP)
Mutual coherence
Array configuration

ABSTRACT

In this paper, we present a new performance guarantee for Orthogonal Matching Pursuit (OMP) in the context of the Direction Of Arrival (DOA) estimation problem. For the first time, the effect of parameters such as sensor array configuration, as well as signal to noise ratio and dynamic range of the sources is thoroughly analyzed. In particular, we formulate a lower bound for the probability of detection and an upper bound for the estimation error. The proposed performance guarantee is further developed to include the estimation error as a user-defined parameter for the probability of detection. Numerical results show acceptable correlation between theoretical and empirical simulations.



## 1. Introduction

Estimating the direction of arrival (DOA) has been a ubiquitous problem in sensor array signal processing for decades [1]. In many applications such as sensor networks, the received signal vector arriving at the antenna elements is sparse. Numerous methods have been proposed to formulate the DOA estimation as a sparse recovery problem [2,3]. A substantial amount of work has been focused on utilizing $\ell_1$ relaxation methods, such as [4–7], for DOA estimation. In this direction, one of the first attempts is the seminal work of Gorodnitsky et al. [8], in which a recursive least-squares algorithm named FOCal Underdetermined System Solver (FOCUSS) is used for source localization. Fuchs [9,10] has formulated the source localization as a sparse recovery problem in the beamspace domain. Cotter [11] combined Multiple Measurement Vectors (MMV) and Matching Pursuit (MP) [12] algorithms to solve the joint-sparse recovery problem in DOA estimation. In [13–15], the $\ell_1$-SVD method combines the Singular Value Decomposition (SVD) step of the subspace algorithms with a sparse recovery method based on $\ell_1$ minimization. Stoica et al. [16] extended this idea by utilizing the sparsity observed in the covariance matrix.

In general, the main disadvantage of $\ell_1$ relaxation methods, as noted in [17], is high computational complexity. When the number of antenna elements becomes large, even the sub-optimal methods such as $\ell_1$-SVD or the covariance-based techniques suffer from high computational and storage complexity. In many applications, memory and computational resources are scarce, hence the aforementioned methods cannot be efficiently implemented. For instance, wearable sensors need ultra-low power and low cost systems that prohibit the use of complex recovery algorithms. A compelling alternative to $\ell_1$ relaxation methods is the family of greedy methods for DOA estimation, which are substantially faster and suitable for efficient implementation on low-power hardware [18–21]. A well-known greedy algorithm is Orthogonal Matching Pursuit (OMP) [22], which has been shown to provide a reasonable trade-off between the computational complexity and the accuracy [23–25].

Despite low computational burden, greedy algorithms have received a surprisingly little attention for DOA estimation. In this direction, Yang et al. [26] have compared MP and Basis Pursuit (BP) [27] for a predefined beam pattern, however, without any theoretical analysis. In [28] and [29], a comparison of OMP and MP with MUSIC [1,30] for DOA estimation is presented. Moreover, Cotter [31] presents a two stage and tree-based OMP method to achieve better accuracy, but without theoretical guarantees. Previous methods have only considered linear arrays of antennas, and the convergence of proposed approaches is not analyzed thoroughly.

In this paper, we present a new theoretical analysis of the OMP algorithm in the context of DOA estimation. Unlike previous work involving performance guarantees for OMP, our analysis considers various parameters such as power variation of different sources (dynamic range of the system), SNR, number of antenna elements, and array configuration, as well as number of sources. Specifically, we will formulate a lower bound for the probability of detection and an upper bound for the estimation error of the received signal.

The paper is organized as follows: We will formulate the problem of DOA estimation as a sparse recovery framework in sec-

* Corresponding author.
*E-mail addresses:* memadi@qti.qualcomm.com (M. Emadi), ehsan.miandji@liu.se (E. Miandji), jonas.unger@liu.se (J. Unger).
[1] Equal contributor.

https://doi.org/10.1016/j.dsp.2018.04.006
1051-2004/

tion 2. In section 3 mutual coherence will be introduced as a parameter related to the array configurations which, along with signal parameters, will be used in Section 4 to determine the probability of detection and the estimation error. Numerical results presented in section 5 demonstrate acceptable correlation to simulation outcomes for a large range of parameters. Finally, the paper will be concluded in section 6.

**Notations** – Vectors and matrices are denoted by boldface lower-case (e.g. $\mathbf{s}$) and bold-face upper-case letters (e.g. $\mathbf{A}$), respectively. Moreover, the elements of vectors and matrices are denoted $\mathbf{s}_n$, and $\mathbf{A}_{n,m}$, respectively. The $j$th column of a matrix, $\mathbf{A}$, is denoted $\mathbf{A}_j$. The transpose and the Moore–Penrose pseudo-inverse are denoted $\mathbf{A}^T$ and $\mathbf{A}^+$, respectively. Given an index set, $\Lambda$, the sub-matrix $\mathbf{A}_\Lambda$ is formed from columns of $\mathbf{A}$ indexed by $\Lambda$. The $\ell_0$ pseudo-norm of a vector $\mathbf{s}$, denoted $\|\mathbf{s}\|_0$, defines the number of non-zero elements. The index set of nonzero elements in $\mathbf{s}$, also known as the support set, is denoted supp($\mathbf{s}$). Consequently, $\|\mathbf{s}\|_0 = |\text{supp}(\mathbf{s})|$, where $|.|$ denotes the set cardinality. Occasionally, the exponential function, $e^x$, is denoted $\exp(x)$.

## 2. Problem definition

In this paper, for the sake of simplicity, we focus on the two-dimensional DOA estimation problem, i.e. we are interested in estimating the azimuth angles of the sources, and not the elevation. Define $\boldsymbol{\phi} = [\phi_1, \ldots, \phi_N]^T$ to be the set of all swept angles and $\boldsymbol{\theta} = [\theta_1, \ldots, \theta_\tau]^T$ to be the set of azimuth angles for $\tau$ sources, where $\tau < N$. Consider $N$ signals $\mathbf{s}_n$, where $n \in \{1, \ldots, N\}$, arriving at $L$ antenna elements. The signal vector $\mathbf{s}$ is defined as follows:

$$\mathbf{s}_n = \begin{cases} \sqrt{p_n} e^{j\psi_n} & \phi_n \in \boldsymbol{\theta}, \\ 0 & \phi_n \notin \boldsymbol{\theta}, \end{cases} \tag{1}$$

where $p_n$ and $\psi_n$ are the received signal power and phase from an illuminator placed at $\phi_n$, respectively. The location of nonzero elements in $\mathbf{s}$ is called the *support* set, which we denote by $\Lambda$. The number of nonzero elements in $\mathbf{s}$ defines the *sparsity* of the signal and is measured using the $\ell_0$ pseudo-norm, denoted $\tau = \|\mathbf{s}\|_0$. From the discussion above it is evident that $\boldsymbol{\theta} = \boldsymbol{\phi}_\Lambda$. We assume that the nonzero elements of the sparse signal $\mathbf{s}_n$ are zero-mean independent random variables with arbitrary distribution. Moreover, it is assumed that the random variables $\mathbf{s}_n$ are bounded. Hence we define

$$s_{\min} = \min(|\mathbf{s}_i|), \quad i \in \Lambda, \tag{2}$$

$$s_{\max} = \max(|\mathbf{s}_i|), \quad i \in \Lambda, \tag{3}$$

as deterministic parameters that are defined based on the requirements of the application at hand.

Let $y_l$, $l \in \{1, \ldots, L\}$, to be the received signal at the port of the $l^{\text{th}}$ antenna. The received signal at the antenna terminals, $\mathbf{y} = [y_1, \ldots, y_L]^T$, can be written as:

$$\mathbf{y} = \mathbf{A}(\phi)\mathbf{s} + \mathbf{w}, \tag{4}$$

where $\mathbf{s} = [\mathbf{s}_1, \ldots, \mathbf{s}_n]^T$ and $\mathbf{w}$ is the additive white Gaussian noise with covariance $\sigma^2\mathbf{I}$. The matrix $\mathbf{A} = [\mathbf{A}_1, \ldots, \mathbf{A}_N] \in \mathbb{C}^{L\times N}$ is often called an *array manifold matrix*, where each column is called a steering vectors. Each of the $N$ steering vectors contains gain and delay information from the $n$th source located at $\phi_n$ to the antennas. For example, elements of the $n$th steering vector for a uniform linear array are [1]

$$\mathbf{A}_n(l) = e^{jl(2\pi d/\lambda)\cos(\phi_n)}, \tag{5}$$

where $\lambda$ is the wavelength, and $d$ is the spacing between antenna elements, and $j^2 = -1$.

Our final goal in the process of DOA estimation can be stated as finding the location of nonzero values in the signal $\mathbf{s}$ from the measurement $\mathbf{y}$. The number of sources is usually much smaller than the total number of swept angles (i.e. $\boldsymbol{\theta}$ is a small subset of $\boldsymbol{\phi}$); hence $\mathbf{s}$ is a sparse vector, making it suitable for sparse signal recovery algorithms. In some applications, such as sensor image processing, in addition to the location of nonzero components, it is required to estimate $p_n$ and $\psi_n$.

## 3. Mutual coherence

Many metrics exists for evaluating the suitability of an array manifold matrix for recovering the support of a sparse signal (i.e. DOA estimation). A few examples are: Mutual Coherence (MC) [32], Cumulative Coherence (CC) [33], Exact Recovery Coefficient (ERC) [34], and Restricted Isometry Constant (RIC) [2]. Among these metrics, RIC achieves tighter bounds, i.e. better performance guarantees for exact recovery. However, computing RIC for arbitrary dictionaries is NP-hard. On the other hand, computing ERC is a combinatorial problem, which is often intractable. A more appealing metric is the MC, which can be computed efficiently and has shown to provide acceptable performance guarantees [35–38]. Our analysis is based on mutual coherence to provide a simple and practical framework for theoretical analysis of OMP in the context of DOA estimation.

The mutual coherence of an array manifold matrix is the absolute cross correlation between its steering vectors [32]:

$$\mu_{a,b}(\mathbf{A}) = \frac{|\langle \mathbf{A}_a, \mathbf{A}_b \rangle|}{\|\mathbf{A}_a\|_2 \|\mathbf{A}_b\|_2}, \tag{6}$$

$$\mu_{\max}(\mathbf{A}) = \max_{1\le a\neq b\le N} \mu_{a,b}(\mathbf{A}). \tag{7}$$

It should be noted that $\|\mathbf{A}_i\|_2 = \sqrt{L}$, for all $i \in \{1, \ldots, N\}$. In what follows, we will calculate the mutual coherence for various array configurations.

Assume $L$ array elements are placed on coordinates $(x_l, y_l)$. Then, MC for an arbitrary array configuration can be formulated as follows

$$\begin{aligned} \mu_{(\phi_i,\phi_j)} &= \frac{1}{L} \left| \langle \mathbf{A}_i, \mathbf{A}_j \rangle \right| \\ &= \frac{1}{L} \left| \sum_{l=1}^{L} e^{-jk_0(x_l(\cos\phi_i - \cos\phi_j) + y_l(\sin\phi_i - \sin\phi_j))} \right|, \end{aligned} \tag{8}$$

where $\mathbf{A}_i$ is the steering vector of the incident wave from direction $\phi_i$ and $k_0$ is the wave number of the received signal. Assume that $\phi_j = \phi_i + \varepsilon$ and define the following:

$$\alpha_{ij} = k_0(\cos\phi_i - \cos\phi_j) = 2k_0 \left[ \sin\left(\phi_i + \frac{\varepsilon}{2}\right) \sin\left(\frac{\varepsilon}{2}\right) \right], \tag{9}$$

$$\beta_{ij} = k_0(\sin\phi_i - \sin\phi_j) = -2k_0 \left[ \cos\left(\phi_i + \frac{\varepsilon}{2}\right) \sin\left(\frac{\varepsilon}{2}\right) \right]. \tag{10}$$

Then from (8) we have that

$$\mu_{(\phi_i,\phi_j)} = L^{-1} \left| \sum_{l=1}^{L} e^{-j\alpha_{ij}x_l} e^{-j\beta_{ij}y_l} \right|. \tag{11}$$

In the rest of this section, we consider the mutual coherence for different array configurations.

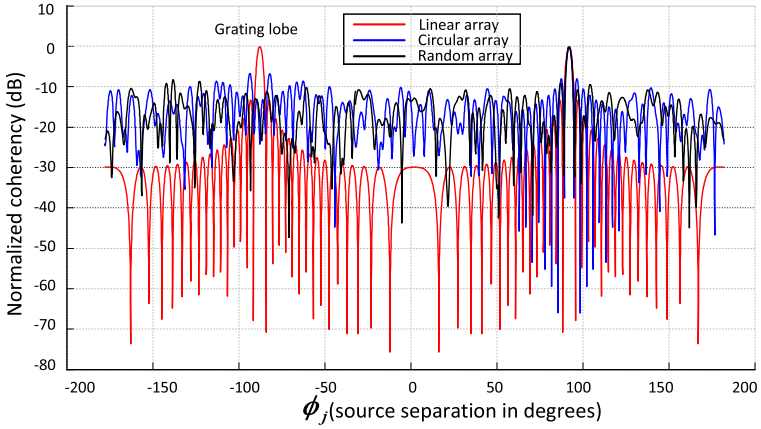


**Fig. 1.** Broad-side mutual coherence.

### 3.1. Uniform Linear Array (ULA)

Consider a ULA of $L$ antenna elements placed at the following coordinates:

$$\begin{cases} x_l = ld, \\ y_l = 0, \end{cases} \tag{12}$$

where $l$ is the antenna index and $d$ is the distance between two adjacent antennas. Using (12), equation (11) can be simplified to:

$$\mu_{i,j}^{\text{ULA}} = \frac{\sin\left(\frac{\alpha_{ij}}{2}Ld\right)}{Ld\sin\left(\frac{\alpha_{ij}}{2}\right)} \tag{13}$$

### 3.2. Uniform Circular Array (UCA)

Consider a UCA of $L$ antennas with the following coordinates:

$$\begin{cases} x_l = R\cos\left(\frac{2\pi}{L}l\right) \\ y_l = R\sin\left(\frac{2\pi}{L}l\right), \end{cases} \tag{14}$$

where $R$ is the radius of UCA. In such a setup, (11) becomes:

$$\mu_{i,j}^{\text{UCA}} = L^{-1}\left|\sum_{l=1}^{L} e^{-j\alpha_{ij}R\cos\left(\frac{2\pi l}{L}\right)} e^{-j\beta_{ij}R\sin\left(\frac{2\pi l}{L}\right)}\right|. \tag{15}$$

For large values of $L$, and defining $m = \frac{l}{L}$, we can estimate (15) as:

$$\begin{aligned} \mu_{i,j}^{\text{UCA}} &\cong \left|\int_0^1 e^{-jR(\alpha_{ij}\cos(2\pi m)+\beta_{ij}\sin(2\pi m))}\,\mathrm{d}m\right| \\ &= \left|J_0\left(R\sqrt{\alpha_{ij}^2+\beta_{ij}^2}\right)\right|, \end{aligned} \tag{16}$$

where $J_0$ denotes the Bessel function.

### 3.3. Uniformly Distributed Array (UDA)

Assume that the coordinates of $L$ antennas are uniformly distributed, i.e.

$$\begin{cases} x_l \sim unif\,(a_x, b_x) \\ y_l \sim unif\,(a_y, b_y), \end{cases} \tag{17}$$

where $(a_x, b_x)$ and $(a_y, b_y)$ denote the boundaries of the uniform distribution in $x$ and $y$ coordinates, respectively. According to the fact that the mutual coherence will also be a random variable, we only consider the expected value of the mutual coherence, defined as follows

$$\mathrm{E}\left\{\mu_{i,j}^{\text{UDA}}\right\} = L^{-1}\left|\sum_{l=1}^{L}\varphi_{x_l}(\alpha_{ij})\times\varphi_{y_l}(\beta_{ij})\right| = \left|\varphi_x(\alpha_{ij})\times\varphi_y(\beta_{ij})\right|, \tag{18}$$

where

$$\varphi_{x_l}(\alpha_{ij}) = \mathrm{E}\{e^{-j\alpha_{ij}x_l}\} = \frac{e^{-j\alpha_{ij}b_x} - e^{-j\alpha_{ij}a_x}}{-j\alpha_{ij}(b_x - a_x)} \triangleq \varphi_x(\alpha_{ij}), \tag{19}$$

$$\varphi_{y_l}(\beta_{ij}) = \mathrm{E}\{e^{-j\beta_{ij}y_l}\} = \frac{e^{-j\beta_{ij}b_y} - e^{-j\beta_{ij}a_y}}{-j\beta_{ij}(b_y - a_y)} \triangleq \varphi_y(\beta_{ij}). \tag{20}$$

Note that in (18) we have dropped the subscript $l$ since $x_l$ and $y_l$, where $l \in \{1, \ldots, L\}$ are assumed to be independent and identically distributed. In the next section, we will use mutual coherence as a metric to derive performance guarantees for OMP.

To numerically demonstrate the effect of different array configurations on coherence, we consider two cases. In the first scenario, we place a source at $\pi/2$ (broadside) and in the second scenario we place it at 0 degrees (end-fire). For both cases, a second source was swept with respect to $\phi_j$, and $\mu_{\max}$ is measured. These scenarios are repeated for different array configurations. The coherence between these arrays for broadside and end-fire cases is shown in Figs. 1 and 2, respectively. We assume 31 antenna elements placed in an $16\lambda \times 16\lambda$ area, where $\lambda$ is the wavelength.

It is evident in Fig. 1 that the linear array has lower side lobes, which implies that the mutual coherence decreases more quickly than the circular and random arrays. However, the linear array suffers from two problems: the grating lobe, see Fig. 1, and the end-fire beamwidth, see Fig. 2. Indeed Fig. 2 shows the high value of the mutual coherence when the first source is placed at zero degrees and the second source becomes close to the first one. In contrast, the circular array shows better mutual coherence at the end-fire angles but worse performance when received signals are far from each other. Random array configurations compromise these effects. One of the major advantages of the random array configuration is the semi-random behavior of mutual coupling between array elements [39,40].

## 4. OMP performance guarantee

The main drawback of the OMP algorithm, and greedy methods in general, is that if the support is estimated incorrectly in one iteration, the error will propagate in the consequent iterations [34].

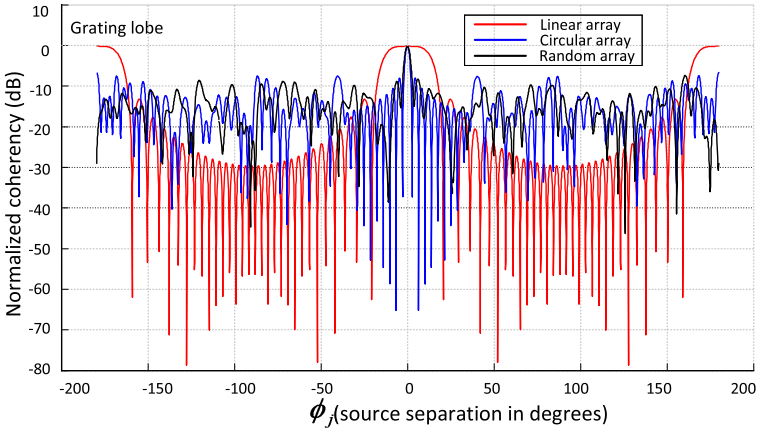


**Fig. 2.** End-fire mutual coherence.

Therefore, in many applications, such as DOA estimation, it is critical to identify the conditions under which this algorithm converges to the correct solution. These conditions should indeed consider signal parameters, i.e. parameters related to the received signal, **y**, as well as the design of the DOA estimation system, i.e. parameters related to the array manifold matrix, **A**.

Below, we present our theoretical results for DOA estimation using OMP. Theorem 1 will present a lower bound for the probability of detection.

**Theorem 1.** *Let* $\mathbf{y} = \mathbf{A}\mathbf{s} + \mathbf{w}$*, where* $\mathbf{A} \in \mathbb{C}^{L\times N}$ *is the array manifold matrix with mutual coherence* $\mu_{\max}$*. Assume that* $\mathbf{w} \sim \mathcal{N}(0, \sigma^2\mathbf{I})$ *and define* $\tau = \|\mathbf{s}\|_0$*. Then, the probability of detection, denoted* $\Pr\{det.\}$*, for DOA estimation using OMP is lower bounded by*

$$\Pr\{det.\} \geq \left(1 - 4N \exp\left(\frac{-(Ls_{\min} - 2\beta)^2}{\frac{16\tau^2L^2\gamma^2}{N} + \frac{8L\gamma(Ls_{\min}-2\beta)}{3\sqrt{2}}}\right)\right) \times \left(1 - N\sqrt{\frac{2\sigma^2}{\pi\beta^2 L}}e^{-\frac{\beta^2}{2L\sigma^2}}\right), \tag{21}$$

*where* $\gamma = \mu_{\max}s_{\max}$ *and* $\beta$ *is a non-negative constant such that* $|\langle \mathbf{A}_j, \mathbf{w}\rangle| \leq \beta$*,* $\forall j \in \{1, \ldots, N\}$*, and* $Ls_{\min} \geq 2\beta$*.*

The proof of Theorem 1 is postponed to Appendix A.

Assuming that OMP correctly identifies the DOA of sources, in some applications we need to accurately estimate the amplitude and phase of the received signals, i.e. the individual values of **s** rather than the location of nonzero entries. We expand the results obtained in Theorem 5.1 of [38] to formulate an upper bound for the absolute error:

$$E_{abs} \triangleq \|\mathbf{s} - \hat{\mathbf{s}}\|_2^2 \leq \frac{\tau\beta^2}{L^2(1 - \mu_{\max}(\tau - 1))^2}, \tag{22}$$

where $\hat{\mathbf{s}}$ is the sparse signal estimated by OMP.

In what follows, using (21) and (22), we derive new bounds for the probability of detection while taking into account DR, SNR, and estimation error. These bounds highlight the importance of each parameter for different applications. We define the DR and SNR of the signal as follows

$$\mathrm{DR} = \left(\frac{s_{\max}}{s_{\min}}\right)^2, \tag{23}$$

$$\mathrm{SNR} = \left(\frac{s_{\min}}{\sigma}\right)^2. \tag{24}$$

Moreover, we define the relative error, denoted $E_{rel}$, as follows

$$E_{rel} \triangleq \frac{E_{abs}}{\sum_{n=1}^{N}\mathbf{s}_n} \leq \frac{E_{abs}}{\tau s_{\min}^2} \leq \frac{\beta^2}{L^2 s_{\min}^2(1 - \mu_{\max}(\tau - 1))^2}. \tag{25}$$

In direction finding systems, we are more interested in identifying the support of the received signal vector and the accuracy of non-zero values in **s** is of lesser importance. Hence, $E_{rel}$ can be rather high. In contrast, if an accurate estimate of the received signals (in terms of phase and amplitude) is required, a small value for $E_{rel}$ is preferable. Evidently, the parameter $E_{rel}$ should be set based on the specific sensor application. Therefore, in what follows we derive "user-friendly" probability of detection bounds based on (21) and a given $E_{rel}$. We approach this problem by considering the two terms in (21) separately. Isolating $\beta$ in (25) we obtain

$$\beta^2 \geq L^2\rho^2 s_{\min}^2 E_{rel}, \tag{26}$$

where $\rho^2 = (1 - \mu_{\max}(\tau - 1))^2$ is defined for notational brevity. Substituting this lower bound for $\beta$ in the second term of (21), and using (23) and (24), we get

$$1 - \frac{N}{L}\sqrt{\frac{2}{\pi\rho^2 E_{rel}L\mathrm{SNR}}}e^{-E_{rel}\rho^2 L\mathrm{SNR}/2}. \tag{27}$$

We need to apply a similar procedure to the first term of (21). Assume that $Ls_{\min} \gg 2\beta$. It will be shown that this is indeed a weak assumption. Without loss of generality we define the upper bound

$$\beta^2 \leq \alpha L\sigma^2 \ll \frac{L^2 s_{\min}^2}{4}, \tag{28}$$

for an arbitrary constant $\alpha \geq 0$. Combining (26) and (28), we obtain a lower bound for $\alpha$:

$$\alpha \geq L\rho^2 \mathrm{SNR} E_{rel}, \tag{29}$$

which together with (28) results in

$$L\rho^2\mathrm{SNR}E_{rel} \leq \alpha \ll \frac{L\mathrm{SNR}}{4}. \tag{30}$$

In other words, we have

$$E_{rel} \ll \frac{1}{2\rho^2} \tag{31}$$

Consequently, given (31), we can use (28) to approximate $(Ls_{\min} - 2\beta)^2$ with $L^2 s_{\min}^2$ in (21). Using this approximation together with (23), (24), and (27), we can rewrite (21) as follows

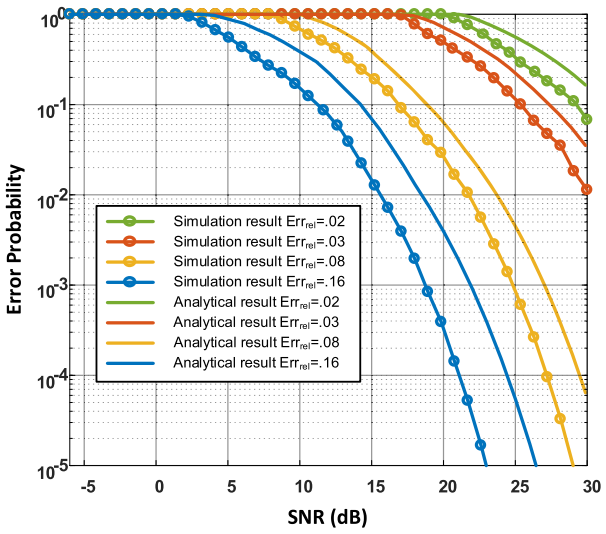


**Fig. 3.** Probability of error vs. SNR for analytical and simulation results. Different values for the relative error $E_{rel}$ is also considered.

$$\Pr\{det.\} \geq \left(1 - 4N \exp\left(\frac{-1}{\frac{16\tau^2\mu_{\max}^2 \mathrm{DR}}{N} + \frac{8\mu_{\max}\sqrt{\mathrm{DR}}}{3\sqrt{2}}}\right)\right) \times \left(1 - \frac{N}{L}\sqrt{\frac{2}{\pi\rho^2 E_{rel} L \mathrm{SNR}}} e^{-E_{rel}\rho^2 L \mathrm{SNR}/2}\right). \quad (32)$$

As it can be seen, the first term of (32) is independent of the noise characteristics of the signal. This term takes into account important signal and array parameters such as DR, $\tau$, and $\mu_{\max}$. On the other hand, SNR and the user-defined relative error are two important parameters in the second term of (32). This is an important distinction of our analysis compared to previous work on OMP performance [38]. Previous work have only considered the second term of (32) as the lower bound for the probability of detection without considering the effect of DR.

Assuming SNR is very high, the second term of (32) becomes negligible. Consequently, the probability of detection is approximately lower bounded by

$$1 - 4N \exp\left(\frac{-1}{\frac{16\tau^2\mu_{\max}^2 \mathrm{DR}}{N} + \frac{8\mu_{\max}\sqrt{\mathrm{DR}}}{3\sqrt{2}}}\right). \quad (33)$$

Equation (33) is particularly useful when for instance the sources are very close to the sensor, leading to a very high SNR, which could also be true when the RCS or transmitted power is very high. As a result, in these cases SNR is very high and the angle separation between the sources, i.e. $\mu_{\max}$, and the power ratio of the sources, i.e. DR, become the predominant parameters.

Assume that $\mu_{\max}$ is very small, which is valid when the number of antenna elements becomes large or when the minimum distance between sources is relatively high. In this case, the probability of detection will be simplified to

$$1 - \frac{N}{L}\sqrt{\frac{2}{L\pi \mathrm{SNR} E_{rel}}} e^{-LE_{rel}\mathrm{SNR}/2}. \quad (34)$$

Since mutual coherence is small, the effect of a high power source next to a low power one will be negligible. Consequently, the probability of detection is dominated by SNR and is independent of DR, which is confirmed by (34).

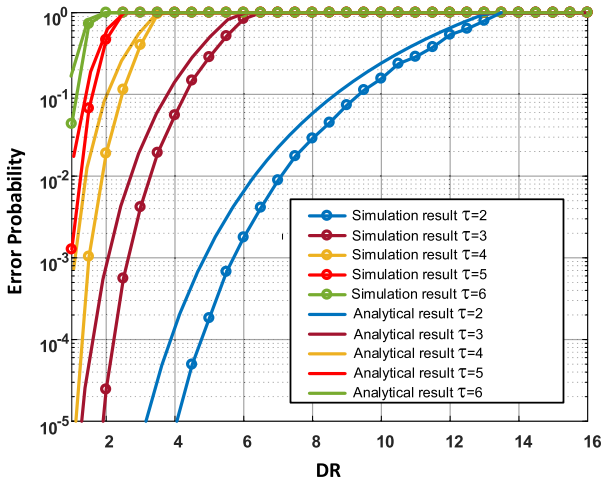


**Fig. 4.** Probability of error vs. DR. For this plot we consider 2 to 6 sources distributed randomly.

## 5. Numerical results

To verify Theorem 1, we compare numerical results of Theorem 1 and simulation results obtained from OMP with respect to SNR, DR, $\tau$, and $E_{rel}$. Ten linear antenna elements randomly distributed in a 7λ distance is assumed. Due to the random distribution, we do not have grating/shadowing lobe and the coupling effect is negligible. For the numerical results we report in this section we use the probability of error. Given the probability of detection defined in 21, the probability of error is defined as $\Pr\{error\} \leq 1 - \Pr\{det.\}$. This conversion facilitates the depiction of the effect of various parameters in the plots.

In Fig. 3, we show the effect of SNR and $E_{rel}$ on the probability of error. For this simulation, only one source was assumed. We set $N = 50$ and swept SNR from $-5$ dB to 30 dB. The iterations of OMP terminate when the residual is less than the predefined $E_{rel}$. To calculate the probability of error, we compare the estimated DOA with the true DOA of the source. If this error becomes higher than $\pi/N$, we assume it is an incorrectly estimated DOA. We perform $5 \times 10^6$ trials of this simulation and calculate the empirical probability of error as the ratio of unsuccessful trials to total number of trials. In each trial, the location of the source was selected uniformly at random. For analytical results, we evaluate (32). As can be seen in Fig. 3, higher $E_{rel}$ will result in lower probability of error and there is acceptable correlation between simulation and analytical results.

The effect of DR and the number of sources ($\tau$) on the probability of error is shown in Fig. 4. For simulation results, we placed 2 to 6 sources with minimum angle separation of $\pi/N$ randomly in space. The relative error is set to $E_{rel} = 0.1$ and the simulation was run $5 \times 10^6$ times. In addition, we assume the SNR is very high (50 dB) and the probability of error was calculated as before. As it can be seen, there is a strong correlation between simulation and analytical results across different parameters. It is clear that when the number of sources become larger (e.g. higher than 4), even for a small value of $DR$, the performance of OMP degrades significantly. In addition, when the power ratio becomes higher than 10, even for two sources the probability of error is very high.

As mentioned in section 4, the array configuration, and hence the mutual coherence, has an important effect on the probability of error. To compare ULA, UCA and UDA, in terms of the probability of error with respect to DR and SNR, we proceed as follows. For ULA and UDA, ten antenna elements in a linear and random configuration are distributed over 7λ distance respectively. For UCA we put ten antenna elements on a circle with 7λ diameter. The

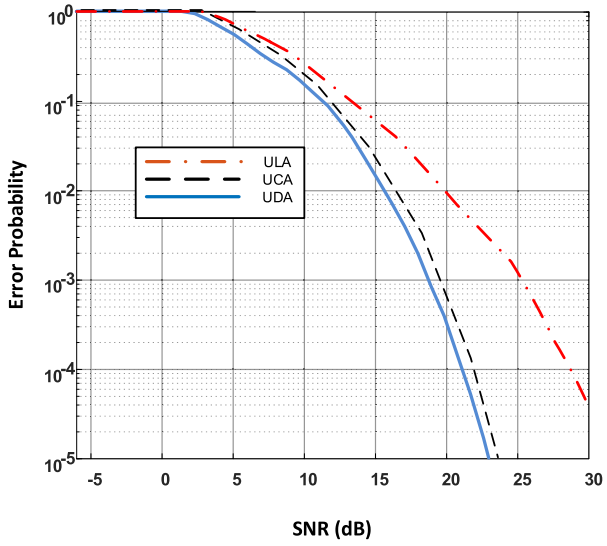


**Fig. 5.** Simulation results for comparing different array configurations with respect to SNR.

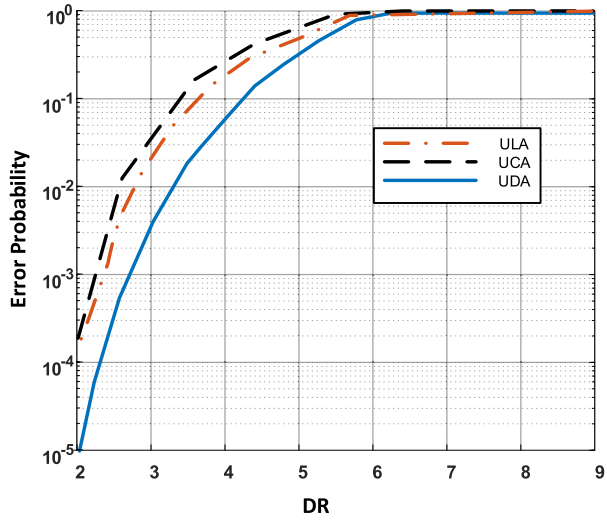


**Fig. 6.** Simulation results for comparing different array configurations with respect to DR.

relative error was set to $E_{rel} = 0.16$, so that the iterations of OMP terminate when the residual relative error is smaller than $E_{rel}$.

In Fig. 5 we compare the performance of different array configurations versus SNR for one source, i.e. $\tau = 1$. The SNR is swept from $-5$ dB to 30 dB. To calculate the probability of error, we compare the estimated DOA with the true DOA of the source. If the error becomes higher than 3.6 degrees, we assume it is an incorrectly estimated DOA. We perform $5 \times 10^6$ trials of this simulation. As before, the location of the source was selected uniformly at random in each trial. It is evident from Fig. 5 that the ULA suffers from grating lobe and it results in worse performance compared to UCA and UDA.

Fig. 6 demonstrates the effect of array configurations on the probability of error with respect to DR. We placed three sources with minimum angle separation of 3.6 degrees randomly in space. The relative error is set to $E_{rel} = 0.1$ and the simulation was run for $5 \times 10^6$ times. On top of that, we assume the SNR is very high (50 dB). As can be seen, the performance of UDA is much better compare to ULA and UCA. Indeed, the performance of ULA is degraded because of the grating lobe, as well as large beam width (high mutual coherence value) in the end fire case. On the other hand, the performance of UCA is also degraded from high mutual coherence when sources are not separated more than 20 degrees (large antenna sidelobes).

## 6. Conclusion

In this paper, for the first time, we presented an analytical discussion for using OMP in DOA estimation using arbitrary array configurations. We showed that the proposed probability of detection is in compliance with simulation results. In addition we proposed several practical formulas with respect to DR, SNR, estimation error, number of sources, angle separation, and the number of antennas. These "user-friendly" bounds can be used as a design methodology for different applications. An interesting venue for future work is to derive new bounds for the probability of detection with respect to the mutual coherence of different array configurations (e.g. see (13), (15), and (18)).

## Appendix A. Proof of Theorem 1

The main tool in the proof of Theorem 1 is the following lemma:

**Lemma 1.** *Let $\mathbf{A} \in \mathbb{C}^{L\times N}$ be the array manifold matrix. Define $\Gamma_j = L^{-1}\left|\langle \mathbf{A}_j, \mathbf{As}+\mathbf{w}\rangle\right|$, for any $j \in \{1,\dots,N\}$, where $\mathbf{w} \sim \mathcal{N}(0,\sigma^2\mathbf{I})$, $\|\mathbf{s}\|_0 = \tau$, and the nonzero elements of $\mathbf{s}$ are centered complex valued random variables. Assume that $|\langle \mathbf{A}_j, \mathbf{w}\rangle| \le \beta$, for all $j \in \{1,\dots,N\}$. Then for some constant $\xi \ge 0$, such that $\xi \ge \frac{\beta}{L}$, the following inequality holds:*

$$\Pr\left\{\Gamma_j \ge \xi\right\} \le 4\exp\left(\frac{-\left(\xi-\frac{\beta}{L}\right)^2}{4\left(N^{-1}\tau^2\mu_{\max}^2 s_{\max}^2 + \frac{\mu_{\max}s_{\max}(\xi-\frac{\beta}{L})}{3\sqrt{2}}\right)}\right), \tag{A.1}$$

**Proof.** Expanding $\Gamma_j$, it is straightforward to show that:

$$\begin{aligned}\Gamma_j &= L^{-1}\left|\langle \mathbf{A}_j, \mathbf{As}+\mathbf{w}\rangle\right| \\ &= L^{-1}\left|\sum_{l=1}^{L}\mathbf{A}_{l,j}^*\left(\sum_{n=1}^{N}\mathbf{A}_{l,n}\mathbf{s}_n + \mathbf{w}_l\right)\right| \\ &= \left|\sum_{n=1}^{N}\left\{L^{-1}\sum_{l=1}^{L}\mathbf{A}_{l,j}^*\mathbf{A}_{l,n}\mathbf{s}_n + \frac{1}{LN}\sum_{l=1}^{L}\mathbf{A}_{l,j}^*\mathbf{w}_l\right\}\right|.\end{aligned} \tag{A.2}$$

From (6) we have that

$$\mu_{j,n} = \frac{\sum_{l=1}^{L}\mathbf{A}_{l,j}^*\mathbf{A}_{l,n}}{\sqrt{L}\sqrt{L}}. \tag{A.3}$$

Combining (A.2) and (A.3) we get

$$\Gamma_j = \left|\sum_{n=1}^{N}\left\{\mu_{j,n}\mathbf{s}_n + \frac{1}{LN}\langle \mathbf{A}_j, \mathbf{w}\rangle\right\}\right|, \tag{A.4}$$

and therefore we have

$$\Pr\left\{\Gamma_j \ge \xi\right\} \le \Pr\left\{\left|\sum_{n=1}^{N}\mu_{j,n}\mathbf{s}_n\right| + \left|\frac{1}{LN}\sum_{n=1}^{N}\langle \mathbf{A}_j, \mathbf{w}\rangle\right| \ge \xi\right\} \tag{A.5}$$

$$\le \Pr\left\{\left|\sum_{n=1}^{N}\mu_{j,n}\mathbf{s}_n\right| \ge \xi - \frac{\beta}{L}\right\}. \tag{A.6}$$

Given that $\mathbf{s}_n$ are complex random variables, equation (A.6) can be upper bounded by

$$\Pr\left\{\Gamma_j \geq \xi\right\} \leq \Pr\left\{\left|\sum_{n=1}^{N} \mathrm{Re}\{\mu_{j,n}\mathbf{s}_n\}\right| \geq \frac{\xi - \frac{\beta}{L}}{\sqrt{2}}\right\} + \Pr\left\{\left|\sum_{n=1}^{N} \mathrm{Im}\{\mu_{j,n}\mathbf{s}_n\}\right| \geq \frac{\xi - \frac{\beta}{L}}{\sqrt{2}}\right\}. \tag{A.7}$$

Our goal is to calculate an upper bound for the right-hand side of (A.7). For this purpose we use the Bernstein inequality [41]. According to Bernstein inequality if $\mathbf{x}_n$ are real-valued centered and independent random variables, where $\Pr\{|\mathbf{x}_n| \leq c\} = 1$ and $\mathrm{E}\{\mathbf{x}_n^2\} \leq \nu$, then we have

$$\Pr\left\{\left|\sum_{n=1}^{N} \mathbf{x}_n\right| \geq \xi\right\} \leq 2\exp\left(\frac{-\xi^2}{2\left(N\nu + \frac{c\xi}{3}\right)}\right) \tag{A.8}$$

It is obvious that the real-valued variables $\mathrm{Re}\{\mu_{j,n}\mathbf{s}_n\}$ and $\mathrm{Im}\{\mu_{j,n}\mathbf{s}_n\}$ in (A.7) are independent centered random variables because of our assumption on $\mathbf{s}_n$. Additionally, the following inequalities hold

$$|\mathrm{Re}\{\mu_{j,n}\mathbf{s}_n\}| \leq |\mu_{j,n}\mathbf{s}_n| \leq \mu_{\max}s_{\max}, \tag{A.9}$$

$$\mathrm{E}\left\{\mathrm{Re}\{\mu_{j,n}\mathbf{s}_n\}^2\right\} \leq \mathrm{E}\left\{|\mu_{j,n}\mathbf{s}_n|^2\right\} \leq \frac{1}{N}\sum_{n=1}^{N}|\mu_{j,n}|^2\mathrm{E}\{|\mathbf{s}_n|^2\} \leq \frac{\tau}{N}\mu_{\max}^2 s_{\max}^2. \tag{A.10}$$

Indeed the same inequalities hold for $\mathrm{Im}\{\mu_{j,n}\mathbf{s}_n\}$. Hence we can apply the Bernstein inequality on both terms on the right-hand side of (A.7). We obtain

$$\Pr\left\{\Gamma_j \geq \xi\right\} \leq 4\exp\left(\frac{-\left(\frac{\xi-\frac{\beta}{L}}{\sqrt{2}}\right)^2}{2\left(\sum_n \mathrm{E}\left\{\mathrm{Re}\{\mu_{j,n}\mathbf{s}_n\}^2\right\} + \frac{\mu_{\max}s_{\max}(\xi-\frac{\beta}{L})}{3\sqrt{2}}\right)}\right) \tag{A.11}$$

$$\leq 4\exp\left(\frac{-\left(\xi-\frac{\beta}{L}\right)^2}{4\left(\frac{\tau^2}{N}\mu_{\max}^2 s_{\max}^2 + \frac{\mu_{\max}s_{\max}(\xi-\frac{\beta}{L})}{3\sqrt{2}}\right)}\right), \tag{A.12}$$

which completes the proof. □

**Proof of Theorem 1.** Define $\Lambda_0$ as the true support of $\mathbf{s}$. It has been shown in [42] that assuming $|\langle\mathbf{A}_j, \mathbf{w}\rangle| \leq \beta$, OMP estimates the true support if:

$$\min_{j\in\Lambda_0} |L^{-1}\langle\mathbf{A}_j, \mathbf{A}_{\Lambda_0}\mathbf{s}_{\Lambda_0} + \mathbf{w}\rangle| \geq \max_{k\notin\Lambda_0} |L^{-1}\langle\mathbf{A}_k, \mathbf{A}_{\Lambda_0}\mathbf{s}_{\Lambda_0} + \mathbf{w}\rangle|, \tag{A.13}$$

where $\mathbf{A}_{\Lambda_0}$ is formed using the columns of $\mathbf{A}$ indexed by the support set $\Lambda_0$. Using the triangle inequality, we can rewrite the term on the left-hand side of (A.13) as:

$$\begin{aligned}&\min_{j\in\Lambda_0} |L^{-1}\langle\mathbf{A}_j, \mathbf{A}_{\Lambda_0}\mathbf{s}_{\Lambda_0} + \mathbf{w}\rangle| \\ &= \min_{j\in\Lambda_0} \left|\mathbf{s}_j + L^{-1}\langle\mathbf{A}_j, \mathbf{A}_{\Lambda_0\setminus\{j\}}\mathbf{s}_{\Lambda_0\setminus\{j\}} + \mathbf{w}\rangle\right| \\ &\geq \min_{j\in\Lambda_0} \left|\mathbf{s}_j\right| - \max_{j\in\Lambda_0} \left|L^{-1}\langle\mathbf{A}_j, \mathbf{A}_{\Lambda_0\setminus\{j\}}\mathbf{s}_{\Lambda_0\setminus\{j\}} + \mathbf{w}\rangle\right|.\end{aligned} \tag{A.14}$$

From (A.13) and (A.14), we can say that the OMP converges to the true support if:

$$\begin{cases} \max_{k\notin\Lambda_0}\{\Gamma_k\} < \min_{j\in\Lambda_0}\dfrac{|\mathbf{s}_j|}{2}, \\ \max_{j\in\Lambda_0}\left|L^{-1}\langle\mathbf{A}_j, \mathbf{A}_{\Lambda_0\setminus\{j\}}\mathbf{s}_{\Lambda_0\setminus\{j\}} + \mathbf{w}\rangle\right| < \min_{j\in\Lambda_0}\dfrac{|\mathbf{s}_j|}{2}. \end{cases} \tag{A.15}$$

Using (A.15) we can define the probability of error for OMP as:

$$\begin{aligned}&\Pr\{\text{error}\} = \\ &\Pr\left\{\max_{j\in\Lambda_0}\left|L^{-1}\langle\mathbf{A}_j, \mathbf{A}_{\Lambda_0\setminus\{j\}}\mathbf{s}_{\Lambda_0\setminus\{j\}} + \mathbf{w}\rangle\right| \geq \frac{s_{\min}}{2}\right\} \\ &+ \Pr\left\{\max_{k\notin\Lambda_0}\{\Gamma_k\} \geq \frac{s_{\min}}{2}\right\},\end{aligned} \tag{A.16}$$

with an upper bound defined as:

$$\begin{aligned}&\Pr\{\text{error}\} \leq \\ &\sum_{j\in\Lambda_0}\Pr\left\{L^{-1}\left|\langle\mathbf{A}_j, \mathbf{A}_{\Lambda_0\setminus\{j\}}\mathbf{s}_{\Lambda_0\setminus\{j\}} + \mathbf{w}\rangle\right| \geq \frac{s_{\min}}{2}\right\} \\ &+ \sum_{k\notin\Lambda_0}\Pr\left\{\Gamma_k \geq \frac{s_{\min}}{2}\right\}.\end{aligned} \tag{A.17}$$

For the first term on the right-hand side of (A.17), excluding the summation over all indices in the support, from Lemma 1 we have:

$$\Pr_{j\in\Lambda_0}\left\{L^{-1}\left|\langle\mathbf{A}_j, \mathbf{A}_{\Lambda_0\setminus\{j\}}\mathbf{s}_{\Lambda_0\setminus\{j\}} + \mathbf{w}\rangle\right| \geq \frac{s_{\min}}{2}\right\} \leq \underbrace{4\exp\left(\frac{-(Ls_{\min} - 2\beta)^2}{16N^{-1}(\tau-1)^2L^2\gamma^2 + \frac{8L\gamma(Ls_{\min}-2\beta)}{3\sqrt{2}}}\right)}_{\mathrm{P}_1}, \tag{A.18}$$

where we have defined $\gamma = \mu_{\max}s_{\max}$ for notational brevity. Note that unlike Lemma 1 where $\Gamma_j$ was written as sum of $N$ random variables, in (A.18) the matrix $\mathbf{A}$ is only supported on $\Lambda_0 \setminus \{j\}$, i.e. all the indices in the true support excluding $j$. Therefore the term $(\tau - 1)$ appears in the denominator of (A.18) after applying the Bernstein inequality.

Similarly, for the second term on the right-hand side of (A.16) we can show that

$$\Pr_{k\notin\Lambda_0}\left\{\Gamma_k \geq \frac{s_{\min}}{2}\right\} \leq \underbrace{4\exp\left(\frac{-(Ls_{\min} - 2\beta)^2}{16N^{-1}\tau^2L^2\gamma^2 + \frac{8L\gamma(Ls_{\min}-2\beta)}{3\sqrt{2}}}\right)}_{\mathrm{P}_2}, \tag{A.19}$$

where we used the fact that the matrix $\mathbf{A}$ in $\Gamma_k$ is supported on $\Lambda_0$, see right-hand side of (A.13). Using the upper bounds $\mathrm{P}_1$ and $\mathrm{P}_2$ obtained in (A.18) and (A.19), we can rewrite (A.17) as

$$\Pr\{\text{error}\} \leq \tau\mathrm{P}_1 + (N-\tau)\mathrm{P}_2, \tag{A.20}$$

$$\leq N\mathrm{P}_2, \tag{A.21}$$

where (A.21) follows since $\mathrm{P}_2 > \mathrm{P}_1$. Since we have assumed that $|\langle\mathbf{A}_j, \mathbf{w}\rangle| \leq \beta$, the probability of error will be the joint probability of the event $\Pr\left\{|\langle\mathbf{A}_j, \mathbf{w}\rangle| \leq \beta\right\}$ and the inverse of (A.21). A lower bound was formulated for $\Pr\left\{|\langle\mathbf{A}_j, \mathbf{w}\rangle| \leq \beta\right\}$ in [42], however when $\mathbf{A}$ has normalized columns. A simple extension of this bound to account for an array manifold matrix with $\|\mathbf{A}_i\|_2 = \sqrt{L}$ yields

$$\Pr\left\{|\langle \mathbf{A}_j, \mathbf{w}\rangle| \le \beta\right\} \ge 1 - \underbrace{\sqrt{\frac{2\sigma^2}{\pi\beta^2 L}} e^{-\frac{\beta^2}{2L\sigma^2}}}_{P_3}. \tag{A.22}$$

Since $|\langle \mathbf{A}_j, \mathbf{w}\rangle| \le \beta$ should hold for all $j \in \{1, \ldots, N\}$, we have

$$\Pr_{j=1,\ldots,N}\left\{|\langle \mathbf{A}_j, \mathbf{w}\rangle| \le \beta\right\} \ge (1 - P_3)^N \ge 1 - NP_3. \tag{A.23}$$

Inverting (A.21) and combining the result with (A.23) leads to (21), completing the proof. □

## References


[1] H. Krim, M. Viberg, Two decades of array signal processing research: the parametric approach, IEEE Signal Process. Mag. 13 (4) (1996) 67–94, https://doi.org/10.1109/79.526899.

[2] E.J. Candès, J.K. Romberg, T. Tao, Stable signal recovery from incomplete and inaccurate measurements, Commun. Pure Appl. Math. 59 (8) (2006) 1207–1223, https://doi.org/10.1002/cpa.20124.

[3] X. Wu, W.P. Zhu, J. Yan, Direction of arrival estimation for off-grid signals based on sparse Bayesian learning, IEEE Sens. J. 16 (7) (2016) 2004–2016, https://doi.org/10.1109/JSEN.2015.2508059.

[4] E. Candes, T. Tao, The Dantzig selector: statistical estimation when $p$ is much larger than $n$, Ann. Stat. 35 (6) (2007) 2313–2351, https://doi.org/10.1214/009053606000001523.

[5] H. Mohimani, M. Babaie-Zadeh, C. Jutten, A fast approach for overcomplete sparse decomposition based on smoothed $\ell^0$ norm, IEEE Trans. Signal Process. 57 (1) (2009) 289–301, https://doi.org/10.1109/TSP.2008.2007606.

[6] S. Wright, R. Nowak, M. Figueiredo, Sparse reconstruction by separable approximation, IEEE Trans. Signal Process. 57 (7) (2009) 2479–2493, https://doi.org/10.1109/TSP.2009.2016892.

[7] B. Efron, T. Hastie, I. Johnstone, R. Tibshirani, Least angle regression, Ann. Stat. 32 (2) (2004) 407–499.

[8] I. Gorodnitsky, B. Rao, Sparse signal reconstruction from limited data using FOCUSS: a re-weighted minimum norm algorithm, IEEE Trans. Signal Process. 45 (3) (1997) 600–616, https://doi.org/10.1109/78.558475.

[9] J.-J. Fuchs, Linear programming in spectral estimation. Application to array processing, in: IEEE International Conference on Acoustics, Speech, and Signal Processing, ICASSP-96, vol. 6, 1996, pp. 3161–3164.

[10] J.-J. Fuchs, On the application of the global matched filter to DOA estimation with uniform circular arrays, IEEE Trans. Signal Process. 49 (4) (2001) 702–709, https://doi.org/10.1109/78.912914.

[11] S.F. Cotter, Multiple snapshot matching pursuit for direction of arrival (DOA) estimation, in: 15th European Signal Processing Conference, EUSIPCO 2007, 2007, pp. 247–251.

[12] S. Mallat, Z. Zhang, Matching pursuits with time–frequency dictionaries, IEEE Trans. Signal Process. 41 (12) (1993) 3397–3415, https://doi.org/10.1109/78.258082.

[13] D. Malioutov, M. Cetin, A. Willsky, A sparse signal reconstruction perspective for source localization with sensor arrays, IEEE Trans. Signal Process. 53 (8) (2005) 3010–3022, https://doi.org/10.1109/TSP.2005.850882.

[14] K. Sun, Y. Liu, H. Meng, X. Wang, Adaptive sparse representation for source localization with gain/phase errors, Sensors 11 (5) (2011) 4780–4793, https://doi.org/10.3390/s110504780.

[15] F. Liu, R. Du, Y. Cheng, Z. Sun, LP-W-$\ell_\infty$-SVD algorithm for direction-of-arrival estimation, IEEE Sens. J. 17 (2) (2017) 428–433, https://doi.org/10.1109/JSEN.2016.2627549.

[16] P. Stoica, P. Babu, J. Li, SPICE: a sparse covariance-based estimation method for array processing, IEEE Trans. Signal Process. 59 (2) (2011) 629–638, https://doi.org/10.1109/TSP.2010.2090525.

[17] M. Hyder, K. Mahata, Direction-of-arrival estimation using a mixed $l_{2,0}$ norm approximation, IEEE Trans. Signal Process. 58 (9) (2010) 4646–4655, https://doi.org/10.1109/TSP.2010.2050477.

[18] L. Bai, P. Maechler, M. Muehlberghuber, H. Kaeslin, High-speed compressed sensing reconstruction on FPGA using OMP and AMP, in: 2012 19th IEEE International Conference on Electronics, Circuits, and Systems, ICECS 2012, 2012, pp. 53–56.

[19] H. Rabah, A. Amira, B.K. Mohanty, S. Almaadeed, P.K. Meher, FPGA implementation of orthogonal matching pursuit for compressive sensing reconstruction, IEEE Trans. Very Large Scale Integr. (VLSI) Syst. 23 (10) (2015) 2209–2220, https://doi.org/10.1109/TVLSI.2014.2358716.

[20] M. Emadi, K.H. Sadeghi, A. Jafargholi, F. Marvasti, Co channel interference cancellation by the use of iterative digital beam forming method, Prog. Electromagn. Res. 87 (2008) 89–103, https://doi.org/10.2528/PIER08100403.

[21] M. Emadi, A. Jafargholi, M.H.S. Moghadam, F. Marvasti, New anti-ARM technique by using random phase and amplitude active decoys, Prog. Electromagn. Res. 87 (2008) 297–311, https://doi.org/10.2528/PIER08100404.

[22] Y. Pati, R. Rezaiifar, P.S. Krishnaprasad, Orthogonal matching pursuit: recursive function approximation with applications to wavelet decomposition, in: Conference Record of the Twenty-Seventh Asilomar Conference on Signals, Systems and Computers, vol. 1, 1993, pp. 40–44.

[23] J. Wang, S. Kwon, B. Shim, Generalized orthogonal matching pursuit, IEEE Trans. Signal Process. 60 (12) (2012) 6202–6216, https://doi.org/10.1109/TSP.2012.2218810.

[24] F. Marvasti, A. Amini, F. Haddadi, M. Soltanolkotabi, B.H. Khalaj, A. Aldroubi, S. Sanei, J. Chambers, A unified approach to sparse signal processing, EURASIP J. Adv. Signal Process. 2012 (2012) 44.

[25] Y.C. Eldar, G. Kutyniok (Eds.), Compressed Sensing Theory and Applications, Cambridge University Press, 2012, Cambridge Books Online.

[26] R. Yang, Y. Liu, Q. Wan, W.L. Yang, Compressive direction finding based on amplitude comparison, J. Netw. 6 (3) (2011) 498–504.

[27] S.S. Chen, D.L. Donoho, M.A. Saunders, Atomic decomposition by basis pursuit, SIAM J. Sci. Comput. 20 (1998) 33–61.

[28] G. Karabulut, T. Kurt, A. Yongaçoglu, Angle of arrival detection by matching pursuit algorithm, in: IEEE 60th Vehicular Technology Conference, vol. 1, 2004, pp. 324–328.

[29] G. Karabulut, T. Kurt, A. Yongaçoglu, Estimation of directions of arrival by matching pursuit (EDAMP), EURASIP J. Wirel. Commun. Netw. 2 (2005) 197–205.

[30] K.H.S.S.N. Shahi, M. Emadi, New anti-arm technique by using random phase and amplitude active decoys, Prog. Electromagn. Res. 5 (2008) 135–148, https://doi.org/10.2528/PIER08100403.

[31] S. Cotter, A two stage matching pursuit based algorithm for DOA estimation in fast time-varying environments, in: 15th International Conference on Digital Signal Processing, 2007, pp. 63–66.

[32] D.L. Donoho, M. Elad, Optimally sparse representation in general (nonorthogonal) dictionaries via $\ell^1$ minimization, Proc. Natl. Acad. Sci. USA 100 (5) (2003) 2197–2202, https://doi.org/10.1073/pnas.0437847100, http://www.pnas.org/content/100/5/2197.full.pdf.

[33] J. Tropp, Just relax: convex programming methods for identifying sparse signals in noise, IEEE Trans. Inf. Theory 52 (3) (2006) 1030–1051, https://doi.org/10.1109/TIT.2005.864420.

[34] J. Tropp, Greed is good: algorithmic results for sparse approximation, IEEE Trans. Inf. Theory 50 (10) (2004) 2231–2242, https://doi.org/10.1109/TIT.2004.834793.

[35] P.L. Dragotti, Y.M. Lu, On sparse representation in Fourier and local bases, IEEE Trans. Inf. Theory 60 (12) (2014) 7888–7899, https://doi.org/10.1109/TIT.2014.2361858.

[36] C. Herzet, C. Soussen, J. Idier, R. Gribonval, Exact recovery conditions for sparse representations with partial support information, IEEE Trans. Inf. Theory 59 (11) (2013) 7509–7524, https://doi.org/10.1109/TIT.2013.2278179.

[37] T. Cai, L. Wang, G. Xu, Stable recovery of sparse signals and an oracle inequality, IEEE Trans. Inf. Theory 56 (7) (2010) 3516–3522, https://doi.org/10.1109/TIT.2010.2048506.

[38] D. Donoho, M. Elad, V. Temlyakov, Stable recovery of sparse overcomplete representations in the presence of noise, IEEE Trans. Inf. Theory 52 (1) (2006) 6–18, https://doi.org/10.1109/TIT.2005.860430.

[39] M. Emadi, K. Sadeghi, DOA estimation of multi-reflected known signals in compact arrays, IEEE Trans. Aerosp. Electron. Syst. 49 (3) (2013) 1920–1931, https://doi.org/10.1109/TAES.2013.6558028.

[40] M. Emadi, K. Sadeghi, Coupling compensation for unmatched circular arrays in high-frequency applications, IET Radar Sonar Navig. 6 (8) (2012) 774–780, https://doi.org/10.1049/iet-rsn.2012.0012.

[41] J. Klemelä, Smoothing of Multivariate Data: Density Estimation and Visualization, Wiley Series in Probability and Statistics, Wiley, 2009.

[42] Z. Ben-Haim, Y. Eldar, M. Elad, Coherence-based performance guarantees for estimating a sparse vector under random noise, IEEE Trans. Signal Process. 58 (10) (2010) 5030–5043, https://doi.org/10.1109/TSP.2010.2052460.


**Mohammad Emadi** received his B.Sc. degree from the University of Tehran, Iran, in 2004, and his M.Sc. and Ph.D. degrees from Sharif University of Technology, Tehran, Iran, in 2006 and 2012, respectively, both in electrical engineering. He worked for six years as a lead designer at communication systems group in the Sharif University Research Center to develop wireless communication links and sensors using phased array antennas. He was also a manager of Tolou Research Center at Sharif University, from 2011 to 2012. From 2013 to 2014, he worked as a postdoctoral research associate at Ultra-High-speed Nonlinear Integrated Circuit (UNIC) lab, Cornell University on sub-millimeter wave imaging systems especially for health care applications, where he won the Cornell Electrical and Computer Engineering Innovation Award. Currently, he is working at Qualcomm Inc. in San Jose as a Senior Staff Manager, focusing on low power sensors, WiFi and small cell communication links. He received the Best Researcher of 2009 from the Ministry of Science, and he was also the

recipient of the Silver Medal of the Physics Olympiad (1999) and honored at IEEE Paper Contest in Iran.

**Ehsan Miandji** received his B.Sc. degree from Azad University, Tehran, Iran, in 2008. and his M.Sc. in computer graphics from Linköping University, Sweden in 2012. Currently, he is a Ph.D. student at the Department of Science and Technology, Linköping University, Sweden. His research interests include compressed sensing and dictionary learning, with applications to lightfield imaging and photo-realistic rendering.

**Jonas Unger** is a an associate professor at the Department of Science and Technology at Linköping University. At this position, he is leading the computer graphics and image processing group (13 FTEs) consisting of senior researchers, PhD students and research engineers. The vision of the group is to research and develop new theory and technology for computational imaging by fusing computer graphics, vision and sensors with human perception and machine learning. With a strong foundation in the theoretically oriented research, the group is active within a number of industrial and academic collaborations directed towards development of state-of-the-art applications ranging from 3D-reconstruction of scenes, photorealistic image synthesis and digitization of optical material properties to computer vision for heart surgery and perceptual display algorithms. Unger's research have been published in over 60 journal articles, conference papers and book chapters. He received his PhD from Linköping University, in 2009, became docent, in 2015, and has during and after his PhD spent about two years as a visiting researcher at University of Southern California, USA.